Journal of Non-Crystalline Solids 72 (1985) 345–368
North-Holland, Amsterdam



# SOL → GEL → GLASS: II. PHYSICAL AND STRUCTURAL EVOLUTION DURING CONSTANT HEATING RATE EXPERIMENTS

C.J. BRINKER [1], G.W. SCHERER [2] and E.P. ROTH [1]

[1] *Sandia National Laboratories, Albuquerque, New Mexico 87185, USA*
[2] *Corning Glass works, Corning, New York 14830, USA*

Received 1 August 1984

Porous, multicomponent gels were converted to dense glasses at temperatures less than 700°C and at heating rates ranging from 0.5 to 40°C/min. The results of shrinkage, weight loss and differential scanning calorimetry experiments were used to elucidate mechanisms responsible for gel densification. We propose that: (1) capillary contraction, (2) condensation polymerization, (3) structural relaxation, and (4) viscous sintering are the principal gel densification mechanisms. Condensation–polymerization and structural relaxation result in skeletal densification, the magnitude of which closely accounts for all the observed shrinkage between 150 and 525°C. Viscous sintering is the predominant shrinkage mechanism above 525°C. Due to the complex interdependency of the densification mechanisms, the kinetics of gel densification depend strongly on thermal history and, therefore, general constant heating rate analyses are inappropriate for deriving meaningful kinetic information regarding the gel → glass conversion.

## 1. Introduction

Part I of this trilogy reviewed the concepts of gelation and provided a basis for distinguishing between polymeric gels and colloidal gels [1]. We concluded that for many conditions of alkoxide gel synthesis the gel network is composed of solvated polymeric species rather than dense colloidal particles. Even continued crosslinking during solvent removal does not result in a fully densified skeleton, i.e. the solid phase comprising the gel is of a lower density than the corresponding melt prepared glass. Thus, during the gel → glass conversion, we expect that the gel will continually change to become more highly crosslinked while reducing its free volume (structural relaxation) and surface area (viscous sintering).

Part II examines the physical, chemical and thermodynamic changes which occur during the conversion of desiccated gels to glasses at constant heating rates. Whereas the commonly held opinion is that gel densification is basically a sintering process [2], we propose that four mechanisms are operative during the gel → glass conversion: (1) capillary contraction, (2) condensation polymerization, (3) structural relaxation and (4) viscous sintering [1,3–5]. The temperature at which each of these mechanisms contributes to densification depends on the structure of both the porous and solid phases of the gel (e.g.

the pore size and the skeletal density) as well as the heating rate and prior thermal history.

In this paper we first describe the structural changes which accompany gel densification at a constant heating rate and propose shrinkage mechanisms. Secondly, we examine the heating rate dependence of these changes to elucidate the complex interdependency of the proposed shrinkage mechanisms. Finally, we assess the validity of using general constant heating rate (CHR) shrinkage equations to obtain kinetic information for the gel → glass conversion.

### *1.2. Gel to glass conversion*

Recently there have been increasing numbers of papers describing the densification of gels. Researchers attempting to quantitatively model this conversion have utilized models originally developed to describe the densification of porous ceramic or metallic powders and have met with varying degrees of success depending primarily on the suitability of the model chosen with the particular gel system investigated. It is pertinent to the present study to review several of these previous investigations of the gel to glass conversion.

Decottignies et al. [6] and Jabra et al. [7] synthesized silica and binary silicate glasses by hot pressing powdered gels previously dehydrated at temperatures ranging from 500 to 800°C. In both investigations, the theoretical model of Murray et al. [8] was applied to describe the densification process. This model is based on a viscous flow mechanism as presented in eq. (1):

$$\log(1 - D) = -\frac{3P}{2.3\eta}t + \log(1 - D_i), \tag{1}$$

where $D$ is the relative density ($\rho/\rho_{glass}$; $\rho_{glass}$ is the density of the corresponding melted glass) $D_i$ is the initial relative density, $P$ is the applied pressure, $\eta$ is the viscosity, and $t$ is the pressing time. This equation is derived from a simplification of the model developed by Mackenzie and Shuttleworth [9] to describe the viscous sintering of a body with closed pores. The applied pressure in eq. (1) is assumed to be so large that the capillary pressure can be neglected. Decottignies et al., found that eq. (1) described their data on silica only for experiments performed at temperatures greater than 1260°C, for which the relative density ranged from 0.9 to 1. The authors argued that these relatively dense samples had closed pores in keeping with the sintering model; whereas less dense gels had continuous porosity and did not conform to the model. However, they also sintered crushed silica powder and found good agreement with eq. (1) for the whole course of densification. Therefore, the deviations of their results on gels from the theoretical prediction more likely reflect the change in viscosity resulting from loss of water during sintering [3] as suggested by their infrared absorption measurements which showed substantial dehydration accompanying densification. Where eq. (1) was obeyed ($> 1260$°C), both the viscosity and the activation energy for viscous flow were considerably less

than the corresponding values reported for vitreous silica [10]. This reflects a higher hydroxyl content and possibly a lower degree of crosslinking than in a melt-formed silica glass.

Jabra et al. measured shrinkage during constant heating rate experiments (flash-pressing) [7]. They observed that eq. (1) (derived for constant heating rates) was not obeyed at temperatures less than ~ 977°C for 5% $P_2O_5 \cdot 95\%$ $SiO_2$ gels previously dehydrated at 800°C. In fact, the apparent viscosity determined at ~ 727°C was over an order of magnitude less than predicted by extrapolation of their high temperature data assuming Arrhenius behavior. Typically, such an extrapolation will *underestimate* the low temperature viscosity because of the upward curvature of a plot of $\ln \eta$ versus $1/T$. Therefore, the unusually low viscosities at low temperatures must result from higher hydroxyl content and possibly from other structural disruptions retained from the gel. These results along with those of Decottignies et al. demonstrate the significant influences of gel structure, e.g. the degree of crosslinking, on the kinetics of viscous sintering.

Nogami and Moriya prepared acid (HCl) and base ($NH_4OH$) catalyzed silica gels from tetraethylorthosilicate (TEOS) using 10 mol. $H_2O$ per mol. of silicon [11]. Transmission electron microscopy (TEM) showed the desiccated form of the base catalyzed polymers to be distinctly globular (or particle-like), whereas the desiccated acid catalyzed gels were featureless. Frenkel's model for initial stage viscous sintering of spherical particles [12] was applied to the isothermal shrinkage data obtained for base catalyzed gels:

$$\Delta l/l_0 = (3\gamma/4\alpha\eta)t, \tag{2}$$

where $l_0$ is the original length of the sample, $\Delta l$ is the change in length at any time, $t$, $\alpha$ is the particle radius, $\eta$ is the viscosity, and $\gamma$ is the surface free energy. Although the base catalyzed gels continuously loss weight up to ~ 1200°C, Frenkel behavior was observed for the initial few minutes of shrinkage at temperatures between 1052 and 1080°C where gel densities ranged from about 1.0 to 2.2 g $cm^{-3}$. Values of $\eta$ determined for each isothermal experiment by use of eq. (2) were consistently less than the corresponding values reported for fused silica (presumably due to the high water contents of these gels); however, the apparent activation energy for viscous flow was calculated to be 170 kcal $mol.^{-1}$ which is quite comparable to the value generally reported for melt-formed $SiO_2$ [9]. This apparent contradiction is difficult to resolve.

Because spherical particles were not evident in TEM of acid catalyzed gels, Nogami and Moriya were unable to apply Frenkel's model. In fact, no existing sintering model satisfactorily explained the isothermal shrinkage data.

In a previous investigation we prepared multicomponent silicate gels under a variety of pH and water conditions [3]. At a heating rate of 2°C $min^{-1}$, gels prepared at pH9 with 12 mol. $H_2O$/mol. alkoxide (HpH12) show only a small amount of densification (attributable to polymerization and structural relaxation) between room temperature and 750°C while gels prepared at pH5 with 5

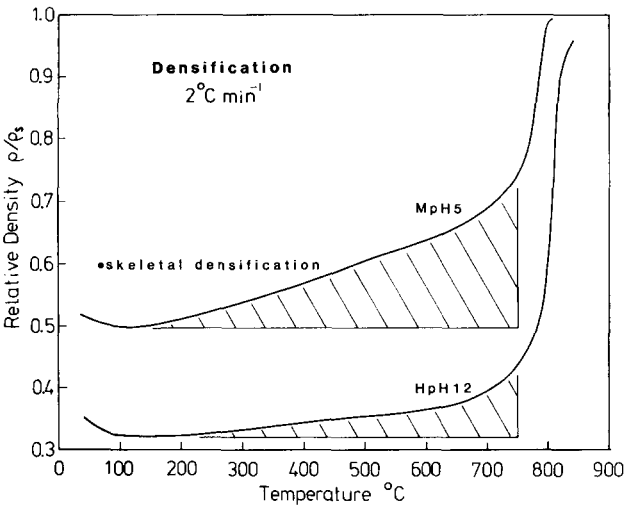


Fig. 1. Densification of multicomponent silicate gels prepared at pH 9 with 12 mol. $H_2O$/mol. alkoxides (HpH12) and at pH 5 with 5 mol. $H_2O$/mol. alkoxides (MpH5). Hatched areas denote skeletal densification as discussed in ref. [4].

mol. $H_2O$/mol. alkoxide (MpH5) densify significantly over this same temperature interval (fig. 1). In addition, shrinkage experiments performed at $T > 750°C$, where viscous sintering was postulated to be the predominant shrinkage mechanism, show that the viscosity of MpH5 gels increases isothermally over two orders of magnitude. Smaller isothermal increases in viscosity occur for HpH12 gels.

In Part I, we discussed how increased concentrations of base and/or water promote crosslinking ultimately resulting in colloid formation, while less highly crosslinked polymers tend to be formed under acid conditions especially with low additions of water [4]. Our previous results and those of Nogami and Moriya are examples of these concepts. In both investigations, the gels prepared under conditions which promote increased crosslinking (increased water and/or base) exhibit densification behavior more similar to that expected for porous, anhydrous glasses (because the structure of the skeletal phase approaches that of a melt-prepared glass); whereas less highly crosslinked, so-called "polymeric" gels (prepared generally under acidic conditions with low additions of water) densified in a manner not predicted by the existing models.

### *1.3. Constant heating rate equation*

Fig. 1 illustrates that it is normally possible to prepare a single gel composition under a variety of conditions which alter both the gel polymer structure and the gel microstructure greatly influencing the kinetics of gel densification. It appears from previous investigations that no single mechanism adequately explains gel densification, therefore, the idea of applying so-called

model-independent constant heating rate shrinkage equations to gel shrinkage data is quite appealing.

Young and co-workers [13,14] studied the kinetics of initial-stage sintering using measurements made at constant heating rates (CHR). They derived equations for shrinkage and shrinkage rate as functions of temperature for the two-sphere geometry and the sintering mechanisms of viscous flow, volume diffusion, and grain boundary diffusion. Woolfrey and Bannister [15] developed more general CHR equations which made no assumptions regarding geometry or densification mechanisms, except that one rate-controlling mechanism predominates.

The equation which applies to CHR conditions was obtained from the general equation for isothermal initial stage singering [16]

$$\frac{\mathrm{d}}{\mathrm{d}t}\left(\frac{\Delta l}{l_0}\right) = \frac{K_0 \exp(-Q/RT)}{(\Delta l/l_0)^n}. \tag{3}$$

This equation assumes that at any combination of shrinkage and temperature the isothermal and nonisothermal shrinkage rates are equal. The activation energy, $Q$ and $n$, a geometric factor, are characteristic of the rate-controlling mechanism. If $Q$, $n$ and the heating rate, $a$, remain constant, eq. (3) may be integrated [15]. Because $Q \gg RT$ the integral may be approximated by:

$$(\Delta l/l_0)^{n+1} = \left[K_0 RT^2(n+1)/aQ\right] \exp(-Q/RT). \tag{4}$$

Values of $K_0$ and $n$ have been tabulated for various sintering mechanisms and geometries [16]. For viscous sintering $K_0$ is constant and $n$ normally equals 0.

In a CHR experiment, the specimen temperature is increased at a constant rate, $a$, and shrinkage or shrinkage rate is determined as a function of temperature. It is apparent from eq. (4) that a plot of $\ln(\Delta l/l_0)$ versus $(1/T)$ gives a straight line of slope $-Q/(n+1)R$. The parameter, $n$, may be evaluated by performing CHR experiments at different heating rates. From eq. (4), a plot of $\ln(\Delta l/l_0)$ versus $\ln(a)$ at constant temperature results in a line of slope $-1/(n+1)$.

For gels, shrinkage generally commences at room temperature, and, depending on the temperature, any of several densification mechanisms might predominate. CHR plots are potentially useful because changes in slope, $[-Q/(n+1)R]$, imply a change in activation energy indicating a change in the predominate shrinkage controlling mechanism. Thus, by using the CHR method it may be possible to obtain mechanistic information for the complete gel → glass conversion. We will show, however, that because there is generally no temperature range in which only one shrinkage mechanism is operative, little kinetic information can be derived from these types of analyses.

## 2. Experimental

Multicomponent silicate gels of nominal oxide composition (wt%) 66 $SiO_2$ · 18 $B_2O_3$ · 7 $Al_2O_3$ · 6 $Na_2O$ · 3 BaO were prepared as described in Part I [4].

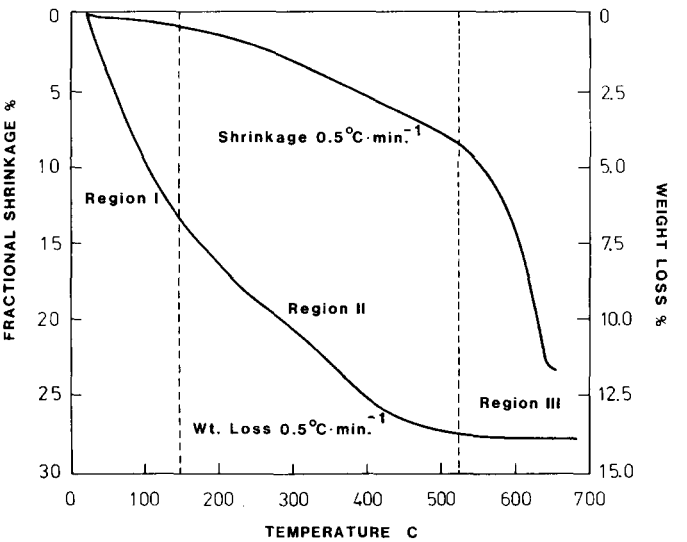


Fig. 2. Linear shrinkage and weight loss measured at 0.5°C/min.

Shrinkage and weight loss were measured at heating rates ranging from 0.5 to 30°C $min^{-1}$ in flowing desiccated air (90 ml $min^{-1}$) using a Theta dual pushrod dilatometer and DuPont 1090 Thermal Analysis system, respectively. Surface area, pore volume, and pore size were determined from analyses of nitrogen adsorption–desorption isotherms (77 K) [1,17]. Samples extracted from constant heating rate experiments were analyzed for hydrogen and carbon by pyrolysis at 2200°C. Differential scanning calorimetry (DSC) experiments were performed in flowing argon at a heating rate of 40°C $min^{-1}$.

## 3. Results and discussion

### *3.1. Shrinkage and weight loss*

Linear shrinkage and weight loss measured at 0.5°C $min^{-1}$ are shown in fig. 2. Three regions are indicated corresponding approximately to the following trends: (I) weight loss without shrinkage (25–150°C), (II) shrinkage proportional to weight loss (150–525°C), and (III) shrinkage without weight loss (> 525°C).

#### *3.1.1. Region I*

According to DTA analyses [2] the weight loss measured in region I is due to desorption of physically adsorbed water and alcohol. The small amount of observed shrinkage in this region results from the increase in surface energy due to desorption. For example, increasing the surface energy, $\gamma$, from 30 erg $cm^{-2}$ (corresponding to a surface saturated with water and alcohol) to 150 erg

$cm^{-2}$ (corresponding to a pure silanol surface [17]) causes an increase in capillary pressure $P$. The resulting linear strain, $\varepsilon$, is [18]:

$$\varepsilon = \frac{(1-\nu)S\rho_s\Delta\gamma}{E}, \tag{5}$$

where $S$ = surface area and $\rho_s$ = skeletal density, $\Delta\gamma$ = change in specific surface energy, and $\nu$ and $E$ are Poisson's ratio and Young's modulus for the glass, respectively. Using the measured value of surface area and the density of the melted glass (496 $m^2\ g^{-1}$ and 2.27 g $cm^{-3}$, respectively [4]) and the typical values $\nu = 0.2$ and $E = 7 \times 11^{11}$ dyn $cm^{-2}$, eq. (6) results in $\varepsilon = 0.15\%$ which is somewhat less than the measured value of 0.6%. Howver, if the solid phase of the gel is not as stiff as the dense glass, its modulus would be lower and the calculated strain would be correspondingly larger. Heat treatments above 150°C will result in dehydration according to:

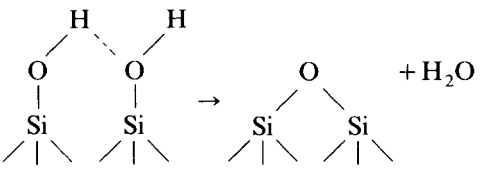


(6)

causing a further increase in surface energy. The maximum additional contraction expected if the surface energy increased to 280 erg $cm^{-2}$ (corresponding approximately to a completely dehydrated surface [17]) is only 0.13%. This additional linear shrinkage would occur between 150°C and 650°C in proportion to the extent of dehydration of the gel surface and, thus, represents a small contribution to the total measured linear shrinkage accompanying densification.

*3.1.2. Region II*

In Region II, weight loss and shrinkage occur concurrently. Weight loss in this region is attributed both to the removal of water as a by-product of polycondensation reactions:

$$\equiv\text{Si-OH HO-Si}\equiv \rightarrow \equiv\text{Si-O-Si}\equiv + H_2O, \tag{7}$$

(which may occur within the skeleton or on the skeletal surface as depicted in eq. (6)) and to the oxidation of carbonaceous residues which were originally present as acetate or unhydrolyzed alkoxy radicals. Fig. 3 shows that although the removal of carbon is essentially complete by 400°C, which corresponds to the upper bound of the associated DTA exotherm [2], hydrogen is removed continuously in this region (150–525°C).

Conceivably, shrinkage in Region II can occur by both increased packing efficiency (e.g. rearrangements of particles comprising the skeleton to higher coordination sites) and skeletal densification (i.e. the approach of the solid

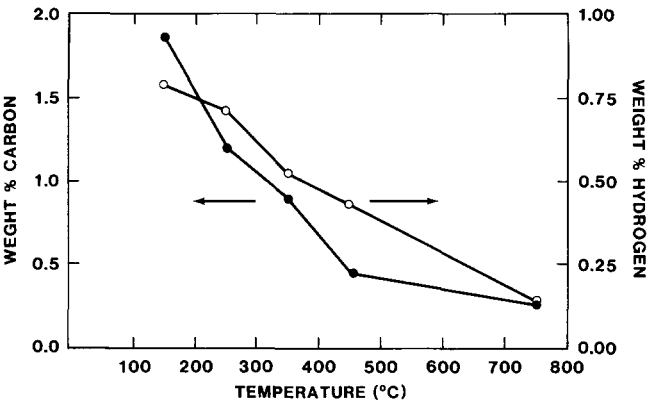


Fig. 3. Carbon and hydrogen contents measured on samples quenched from the indicated temperatures. Initial heat treatments were performed at 2°C/min in flowing air.

phase density toward that of the corresponding melt-prepared glass). As depicted schematically in fig. 4 for the cylindrical array [19] and random close packing geometries, skeletal densification occurs without rearrangement of the original packing configuration, i.e. the matrix shrinks isotropically without changing the coordination number of the units which comprise it. It might also be argued that densification in Region II occurs by a viscous sintering

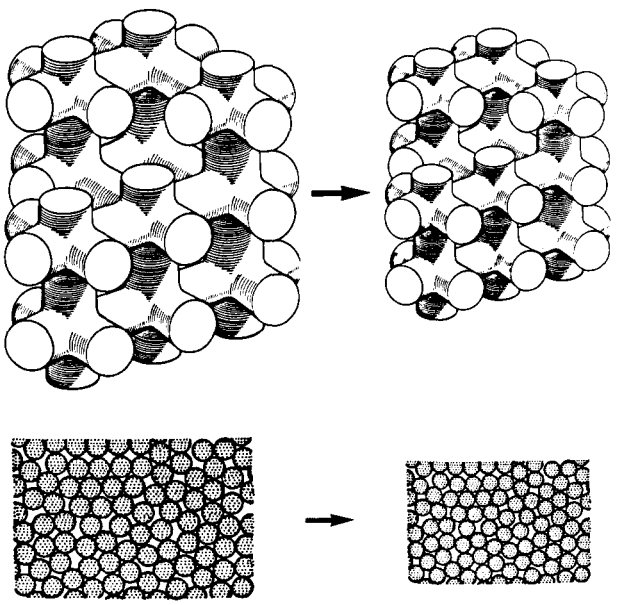

Fig. 4. Schematic depiction of skeletal densification for the cubic cylindrical array and random packing of sphere geometries.

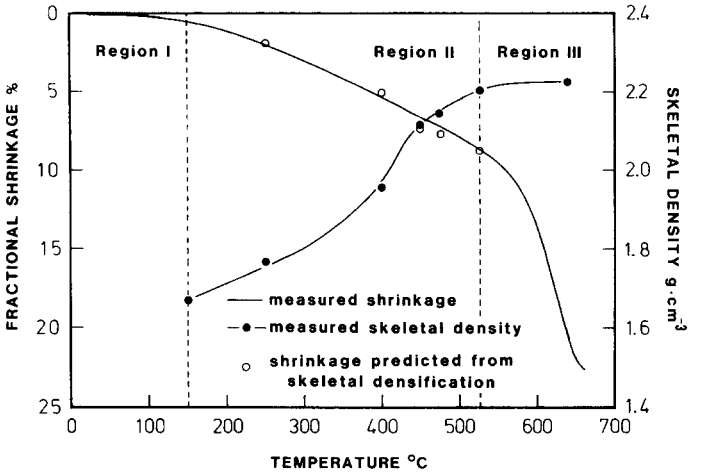


Fig. 5. Linear shrinkage and skeletal density measured for a heating rate of 2°C/min. Open circles represent the shrinkage above 150°C which can be accounted for by the increased skeletal density.

mechanism involving a subset of very small pores. If this were the case, the pores involved would have to be at least an order of magnitude smaller than those participating in sintering in Region III. Thus, pores responsible for viscous sintering in Region II would be ~4 Å in diameter and essentially indistinguishable from free volume. Removal of these "pores" is therefore analogous to structural relaxation.

To distinguish between particle rearrangement and skeletal densification, the skeletal density was calculated from the specific pore volume, $V_p$ and measured bulk density, $\rho_{bulk}$, according to:

$$V_p(\mathrm{cm^3\ g^{-1}}) = \frac{1}{\rho_{bulk}} - \frac{1}{\rho_{skeleton}} \tag{8}$$

by assuming that all the porosity is accessible to the adsorbate molecules [4]. If shrinkage occurs only by rearrangements of particles comprising the skeleton, $\rho_{skeleton}$ remains constant and the change in pore volume is inversely proportional to $\rho_{bulk}$. If skeletal densification occurs, the decrease in pore volume is less than expected from measurements of the bulk density. As shown in fig. 5, the skeletal density increases in Region II from 1.67 (73% of the melt glass density) to 2.20 g cm$^{-3}$ (97% of the melt glass density). This increase closely accounts for all of the measured linear shrinkage, proving that little or none of the shrinkage, in Region II results from particle rearrangements.

For either the cylindrical array model or models based on the packing of spheres, the decrease in surface area which results from skeletal densification equals:

$$\left(\frac{\rho_{skeleton_{(initial)}}}{\rho_{skeleton_{(final)}}}\right)^{2/3} = \frac{S_{final}}{S_{initial}}.$$

Fig. 6 shows that up to ~400°C, the measured surface area decreases

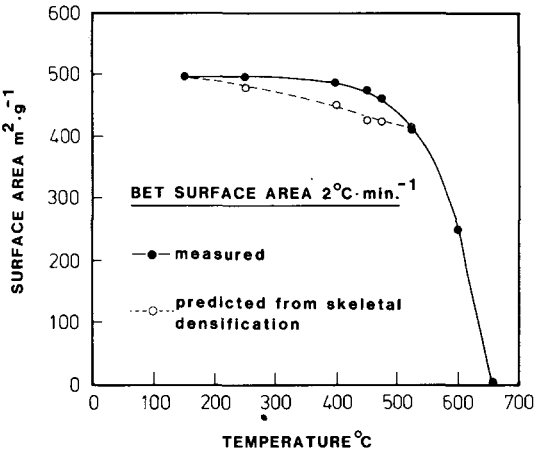


Fig. 6. BET surface area measured for a heating rate of 2°C/min. Open circles represent the expected change in surface area due to increasing skeletal density (fig. 5).

somewhat slower than predicted from the increase in skeletal density using eq.(9). According to Iler [17], this unpredicted behavior may result from "activation" of the surface due to removal of physisorbed and hydrogen bound water and/or combustion of organics both of which make more surface area accessible to the adsorbate gas. Alternatively, skeletal densification may cause roughening of the surface, so that the surface area does not decrease as expected. Above 400°C, the surface area decreases more rapidly than predicted from eq. (9). Conceivably, this results from surface diffusion which causes a reduction in surface area (i.e. smoothing) with no associated densification.

Skeletal densification can occur by both polymerization reactions (e.g. eq. (7)) and structural relaxation, i.e. the approach of the structure toward the configuration characteristic of the metastable liquid. Structural relaxation is achieved by diffusive motion of the polymeric network without expulsion of water or other by-products. It is expected that skeletal densification will make the greatest contribution to shrinkage for weakly crosslinked polymer gels and the smallest contribution for colloidal gels. Evidence supporting this idea is the fact that gels prepared from anhydrous silica particles, formed by flame oxidation of $SiCl_4$, exhibit little low temperature shrinkage [20], whereas gels prepared under conditions which promote the formation of more weakly branched polymers exhibit considerable low temperature shrinkage (e.g. fig. 1 and refs. [4,21,22]) which has been attributed to both condensation and structural relaxation. Further evidence in support of skeletal densification was reported by Tohge et al. [21] who prepared an alkali borosilicate gel completely from alkoxides under more weakly hydrolyzing conditions and measured a large increase in skeletal density (from 1.45 to 2.40 g $cm^{-3}$) which occurred rather continuously over the temperature range: 100 to 550°C.

The contribution of each of the proposed mechanisms (polymerization and structural relaxation) to shrinkage in Region II is difficult to quantify. Al-

though hydrogen is evolved continuously over this temperature interval (fig. 3), there is potentially more than one source of hydrogen; therefore, hydrogen evolution is not necessarily indicative of additional crosslinking. Furthermore, there is limited information on the relationship of density to polymerization, so that, even if the extent of polymerization were known, it would not be possible to accurately predict its effect on densification. With regard to structural relaxation, it is well established for melt-prepared glasses that relaxation processes (which reduce "excess" free volume) occur at temperatures slightly below $T_g$. However, as described in Part I [4], the glass transition temperatures of gels are expected to increase in proportion to the extent of polymerization and structural relaxation. As the skeleton densifies in Region II, the glass transition temperature continually increases, so there is no narrow temperature range in which structural relaxation is predicted to take place. Instead, structural relaxation may contribute to skeletal densification over this complete temperature region.

### *3.1.3. Region III*

Region III (fig. 2) corresponds to a temperature interval where considerable shrinkage occurs with little associated weight loss. This behavior is consistent with a viscous sintering mechanism; however, polymerization and, perhaps, structural relaxation also contribute to the observed shrinkage [3,5]. Evidence supporting a viscous sintering mechanism is presented in fig. 7 where percent linear shrinkage is plotted for a series of borosilicate gels in which the $Na_2O$ content was systematically varied from 6 to 0 wt%. The shrinkage curves show only nominal differences up to ~ 500°C. Above 500°C the temperature at

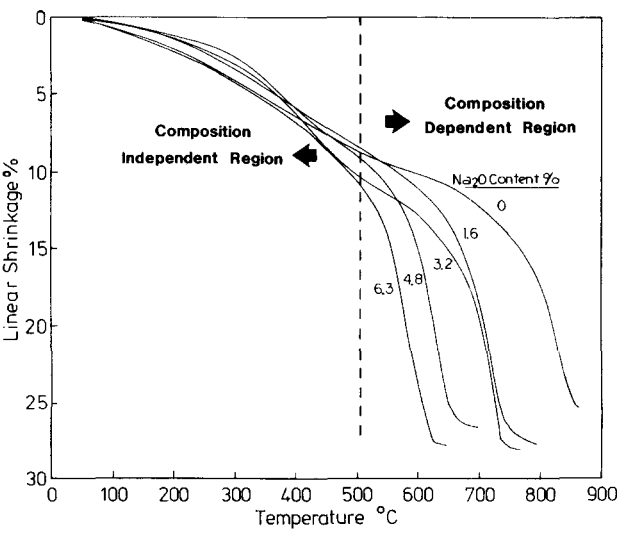


Fig. 7. Linear shrinkage measured at 2°C/min for a series of multicomponent gels in which the $Na_2O$ content varied from 0 to 6.3 wt% (after ref. [4]).

which extensive shrinkage commences scales with decreasing sodium content (decreased $T_g$ of the corresponding melt prepared glasses). For materials with equivalent pore sizes and crosslink densities, this trend (decreasing densification temperature with decreasing $T_g$) suggests that extensive shrinkage commences at a temperature which corresponds to a particular viscosity and, therefore which increases with decreasing sodium content.

Although the skeletal density ($2.23 \pm 0.03$) g cm$^{-3}$ in Region III calculated according to eq. (8) is essentially indistinguishable from that of the corresponding melted glass (2.27 g cm$^{-3}$), the precision of this method is probably insufficient to determine accurately the small increases in skeletal density which may occur concurrently with viscous sintering. This is important because small decreases in free volume cause significant increases in viscosity. For example, Rekhson et al. [23] observed that during structural relaxation in soda-lime silica glasses an increase in density of 0.12% was accompanied by an increase in viscosity by a factor of 3.2. Thus, slight changes in skeletal density (undetectable by our experimental method) could dramatically affect the kinetics of viscous sintering in Region III. In addition, although the associated weight loss is low in this region, polycondensation reactions undoubtedly occur, serving to increase the apparent viscosity. Therefore, although viscous sintering appears to be the predominant shrinkage mechanism in Region III, structural relaxation and polymerization also probably contribute to the observed shrinkage. The implication of having polymerization and structural relaxation accompany sintering will be discussed in more detail in section 3.2 and in Part III [5].

### *3.2. Heating rate dependence*

Because we suspect that the principal mechanisms responsible for gel shrinkage during the gel → glass conversion (polymerization, structural relaxation, and viscous sintering) are kinetically limited and that more than one of these mechanisms can operate concurrently, we expect that gel shrinkage will depend strongly on thermal history. Furthermore, we believe that these mechanisms do not operate independently. For example, it is well known that both decreased crosslinking and increased excess free volume reduce the activation energy for viscous flow. In addition, because structural relaxation (which reduces excess free volume) requires cooperative movements of structural units, we expect that the rate of structural relaxation will have an inverse dependence on the extent of crosslinking. Thus, a complex situation develops in which it is difficult to predict the heating rate dependence of densification. In the remainder of this section, we report on shrinkage, weight loss, DSC, and infrared spectroscopy experiments performed to elucidate the complex interdependency of the proposed shrinkage mechanisms.

Linear shrinkage and percent weight loss are plotted in figs. 8 and 9 for heating rates of 0.5, 2, 10, and 15°C min$^{-1}$. A striking feature of these plots is the virtual absence of a heating rate dependence of shrinkage in Region II

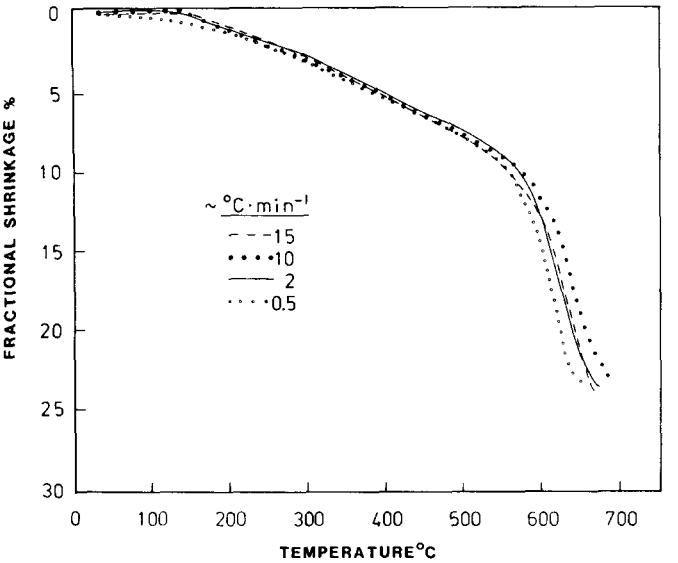


Fig. 8. Linear shrinkage measured at constant heating rates.

whereas there is clearly a heating rate dependence of weight loss. There is generally less than a 0.25% difference in linear shrinkage although the heating rate various by a factor of ~ 30. This behavior may be explained by either of two hypotheses: (1) a single mechanism which is thermodynamically favorable but not kinetically limited for these heating rates is responsible for shrinkage in Region II; or (2) shrinkage in this region is kinetically limited and the rate increases with excess free volume and decreases with increased crosslink density.

In the first case shrinkage occurs by condensation (e.g. eq. (8)), when hydroxylated species come within close proximity to one another. Thermal energy alone is sufficient to bring the reactants to a critical separation distance,

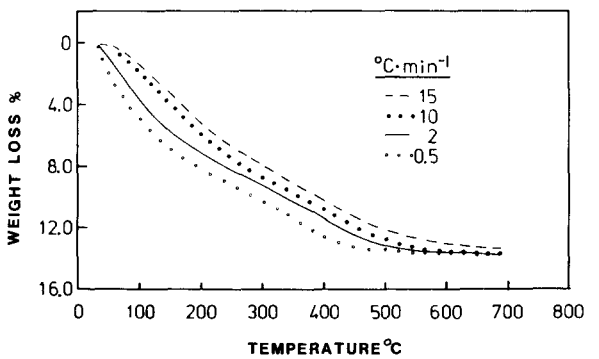


Fig. 9. Weight loss measured at constant heating rates.

at which point condensation occurs spontaneously, causing shrinkage and attendant weight loss. If this hypothesis were correct, the reduced weight loss with increased heating rates could be interpreted as resulting solely from the diffusion-limited evolution of water from the continuous porous network.

If the second hypothesis is correct, shrinkage occurs by polymerization and structural relaxation which are both kinetically limited. Shrinkage, therefore, is proportional to the increment of time spent at each increment of temperature. However, if decreased crosslinking or increased excess free volume increase the rates of condensation and/or relaxation (because structural rearrangements can more readily occur), then the shrinkage rate should be proportional to excess free volume and inversely proportional to the extent of crosslinking. No heating rate dependence would be observed if the increased rates of polymerization and/or relaxation exactly compensated for the reduced times spent at each temperature increment as the heating rate was increased.

To distinguish between these two cases, a series of DSC and thermal gravimetric analysis (TGA) experiments were performed on thin gel wafers initially heated to 525°C in air at heating rates ranging from 2 to 30°C $min^{-1}$ and quenched to room temperature. These quenched samples exhibited virtually identical shrinkages and their surface areas varied by less than 3%. After the initial heat treatment, the gels were brought to thermal equilibrium at 427°C in the DSC and heated at 40°C $min^{-1}$ to 717°C to cause complete densification. The samples were then cooled at 80°C $min^{-1}$ to 427°C (130°C below their $T_g$) and reheated at 40°C $min^{-1}$ to 717°C to observe the glass transition of the densified gels. It was assumed that all physically adsorbed water was removed by 427°C prior to the first DSC scan so that differences in heat capacity above 427°C are due to chemical or physical differences resulting from the initial heat treatments to 525°C. Fig. 10 shows the results.

If shrinkage between 150 and 525°C occurs by a single mechanism, then samples which have undergone identical amounts of shrinkage should be chemically and physically identical. As shown by the substantial differences in the thermograms in fig. 10, this is clearly not the case. At temperatures above

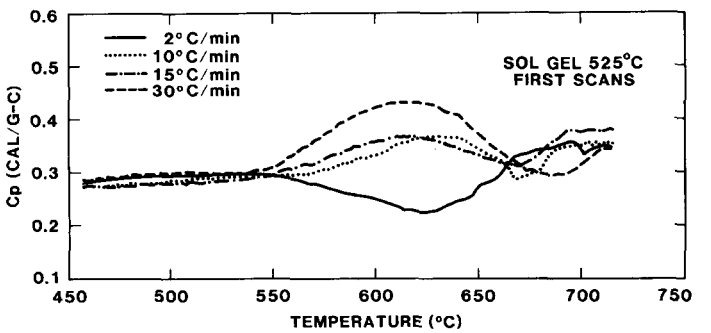


Fig. 10. Heat capacity curves determined at 40°C/min for gels previously heated to 525°C at varying rates.

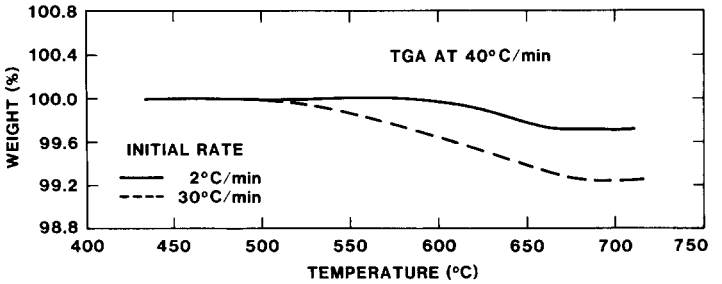


Fig. 11. Weight loss measured at 40°C/min. on samples previously heated to 525°C at 2 and 30°C/min.

525°C, samples previously heated at rates from 10 to 30°C $min^{-1}$ exhibited progressively larger endothermic peaks in the temperature range 525 to 650°C, and progressively larger exothermic peaks in the temperature range 650 to 717°C. The sample previously heated at 2°C $min^{-1}$ shows only an exotherm in the region 525 to 650°C. Companion thermal gravimetric analyses (fig. 11) indicate that these thermodynamic features in the temperature region 525 to 650°C are accompanied by weight loss, the magnitude of which increases with the original heating rate. Repeat DSC runs (fig. 12) show the glass transitions of the fully densified gels.

A Karl Fischer titration of the products evolved during sintering of a similar borosilicate gel [24] proved that all of the weight loss above 350°C could be accounted for by removal of water (a by-product of condensation–polymerization). Hence the TGA results indicate that samples originally heated at higher heating rates to 525°C undergo greater amounts of condensation when heated from 525 to 717°C. By assuming that the hydroxyl contents of the samples originally quenched from 525°C can be calculated from the weight loss (fig. 11) plus the residual [OH] of the fully densified gels, as measured by infrared spectroscopy, we can quantitatively determine the number of non-bridging oxygens in the as-quenched samples. Assuming an extinction coefficient of 56 l

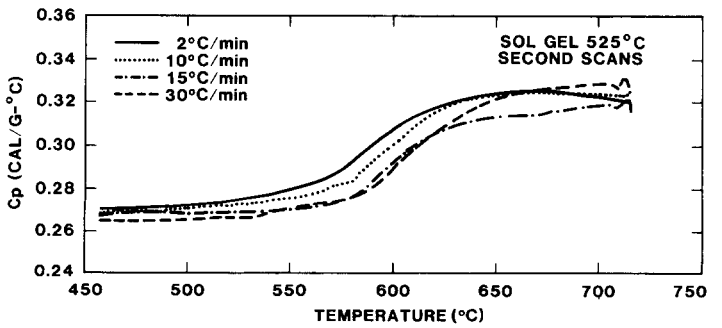


Fig. 12. Repeat heat capacity curves measured at 40°C/min after cooling from 720°C at 80°C/min.

mol.$^{-1}$ cm$^{-1}$ [25] the hydroxyl contents are $5.5 \times 10^{-4}$ and $1.0 \times 10^{-3}$ moles (OH) $g_{gel}^{-1}$ for samples originally heated to 525°C at 2 and 30°C min$^{-1}$, respectively, proving that the differences in total weight loss measured at 525°C (fig. 9) reflect not only the possible diffusion-limited evolution of water but actual differences in the extent of polymerization depending on the initial heating rate.

We have shown that (1) as the heating rate was increased, the extent of crosslinking in the samples quenched from 525°C was reduced, and (2) during the subsequent DSC run, less highly crosslinked gels underwent greater amounts of condensation–polymerization (exhibited greater weight loss). For there to be equal amounts of shrinkage yet different amounts of polymerization, we must conclude that shrinkage in Region II cannot occur by polymerization alone, i.e. at least two shrinkage mechanisms operate concurrently. Therefore, we are led to accept the hypothesis that increased heating rates decrease the extent of polymerizatioin (due to the reduction in time spent at each increment of temperature), but increase the rate of structural relaxation so that there is no apparent heating rate dependence of shrinkage in Region II.

The DSC curves (fig. 11a) can be interpreted as resulting from the exothermic contribution of sintering ($-\Delta S \times \bar{\gamma}$ where $\bar{\gamma}$ = the average surface energy and $\Delta S$ = change in surface area due to densification) plus the endothermic contributions of (1) the vaporization and subsequent heating of water formed as a by-product of polymerization and (2) the heat required to raise the temperature of the skeleton from 525 to 717°C (defined by the heat capacity curves (fig. 12)). In addition, one must take into account the heats of formation of the polymerized silicates. Estimates of the heats of formation of silicates from silicic acids generally show the polymerization process to be weakly exothermic as shown by the following dimerization reaction (eq. (11)) and the net reaction forming silica plus water (eq. (12)):

$$2\,H_4SiO_4 \rightarrow H_6Si_2O_7 + H_2O\ \Delta H_{f\,298\,K} = -17\ \text{kJ mol.}^{-1}, \tag{11}$$

$$H_4SiO_4 \rightarrow SiO_2 + 2H_2O\ \Delta H_{f\,298\,K} = -15\ \text{kJ mol.}^{-1}. \tag{12}$$

However, if some "defective" silicates are formed, the net polymerization process could be endothermic. For example, from molecular orbital calculations, Gibbs has shown that the heat of formation of an edge-sharing silicate dimer is +210 kJ mol.$^{-1}$ [26]:

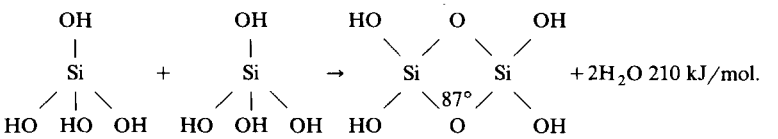


Morrow [27] has proposed the formation of this species during the latter stages of dehydration of colloidal silica surfaces at $T \geq 500$°C to account for new IR absorption bands. Thus, because all silica tetrahedra are within ~ 25 Å of a

surface after heating to 525°C (assuming the gel to be composed of randomly-oriented, cylindrical porosity), the gel structure is dominated by surface species and it is likely that crosslinking, resulting from dehydration of the surface or from condensation reactions near the surface, also results in the formation of some metastable, "energetic" silicate species. Taking into account the change in surface area, the heat of vaporization of water and the heat capacity of the skeleton, it was not possible to account for the magnitude of the endothermic DSC peaks without assuming the net contribution of the heat of formation of Si–O–Si bridges to be positive. Therefore, the progressively larger endotherms which occur with increased heating rates may be interpreted as resulting principally from the progressively larger endothermic contributions of polymerization (and to a lesser extent vaporization) causing the exotherm expected from sintering to be completely obscured at heating rates greater than 2°C $min^{-1}$.

Because of the large strain energy associated with edge sharing polyhedra, it is expected that heating above $T_g$ would cause their dissociation into apex shared polyhedra. This dissociation and reformation would be exothermic and may explain the exotherms which are observed in the temperature interval 650 to 717°C. The integrated areas of the exothermal peaks are considerably less than those of the endotherms suggesting that due to kinetic limitations, complete dissociation may not occur until well above $T_g$.

The heat capacity curves of the densified gels (fig. 12) show a trend of increasing $T_g$ with increased heating rates. IR analyses of these dense gels show that this increase in $T_g$ results in part from decreased residual [OH] contents. This suggests that as the extent of polymerization is reduced in Region II, the subsequent rate of polymerization is increased in Region III (at a heating rate of 40°C/min). Thus, even the structures of fully densified gels depend in a complex fashion on previous thermal history.

### *3.3. Constant heating rate analyses*

In the final section of this paper we attempt to derive kinetic information regarding gel densification by utilizing a modeless, CHR equation developed by Woolfrey and Bannister [15] and an equation developed by Scherer to describe the viscous sintering of a cylindrical cubic array [19]. As stated previously, CHR analyses are potentially attractive because they may be model-independent and because kinetic information can be quickly obtained from a minimum number of experiments. The following discussion, however, illustrates that these analyses are generally inappropriate for obtaining meaningful kinetic information on gels.

Fig. 13 shows $\ln \Delta l/l_0$ versus $1/T$ for Regions II and III in accordance with eq. (4). Because the slope of this plot is predicted to be proportional to an activation energy [15], this figure suggests that one shrinkage mechanism predominates below 400°C and a different shrinkage mechanism (i.e. a mechanism with a different activation energy) predominates above ~ 550°C. From

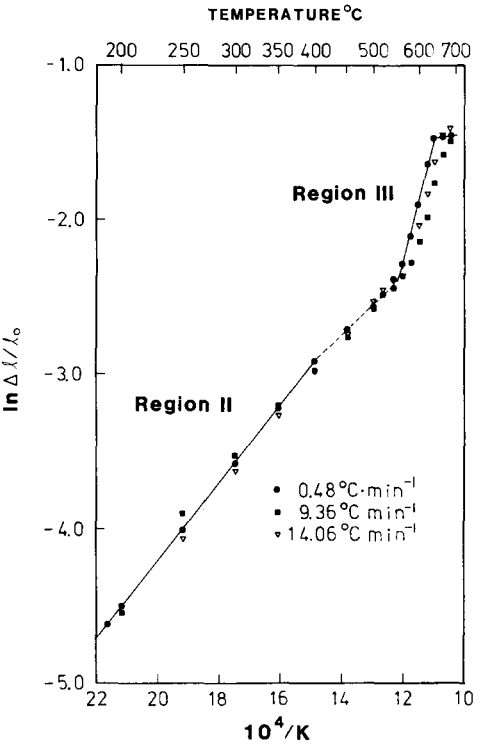


Fig. 13. Ln shrinkage versus $1/T$(K) plots at varying heating rates. Lines were drawn to show changes in slope for the 0.48°C/min. heating rate.

our previous discussion, it is likely that viscous sintering is the predominant shrinkage mechanism above 550°C, and condensation–polymerization is the predominant shrinkage mechanism below 400°C. As shown by the weight loss and skeletal densification curves (figs. 9 and 5 respectively), the temperature interval 400–500°C represents a region where considerable skeletal densification occurs with little associated weight loss (especially for the lowest heating rate). This suggests that structural relaxation, in which the skeleton densifies without expulsion of water, is the predominant shrinkage mechanism in this temperature interval. Structural relaxation is characterized by a different activation energy and, therefore may account for the observed change in slope in fig. 13.

In Region III where viscous sintering is expected to be the predominant shrinkage mechanism, it should be possible, according to the CHR equation of Woolfrey and Bannister [15] to derive kinetic information such as the viscosity and the activation energy for viscous flow. Eq. (4) describes initial stage sintering for a wide variety of geometrical models and shrinkage mechanisms. It predicts that the slope in Region III (fig. 12) equals $-Q/(n+1)R$ where, for a viscous sintering mechanism, $Q$ equals the activation energy for viscous flow and $n$ equals 0. A plot of $\ln(\Delta l/l_0)$ versus $1/T$(K) derived for the

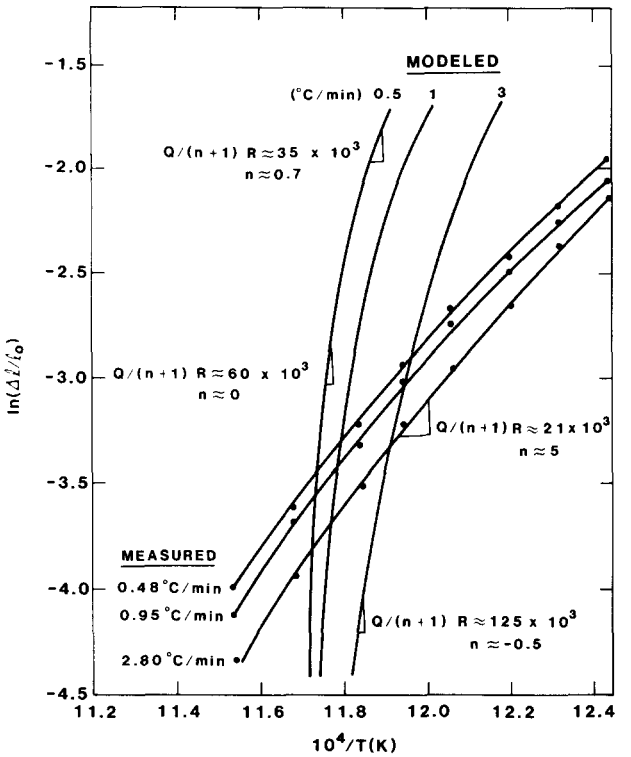


Fig. 14. Ln shrinkage versus $1/T$(K) plots for Region III. Solid lines are predicted by the cylindrical cubic array model and dotted lines present the measured values assuming $\rho/\rho_0 = 0$ at the beginning of Region III.

cylindrical array model [19] is shown in fig. 14 for 3 different heating rates. These plots were obtained by assuming the initial relative density, $\rho_0/\rho_s$, equaled 0.5, the initial cube dimension, $l_0$, equaled 50 Å, the surface energy, $\gamma$, equaled 280 erg $cm^{-2}$, the viscosity, $\eta$, at the glass transition temperature (560°C) equaled $10^{13}$ P, and $Q/R$ equaled $60 \times 10^4$ (K). These assumptions were based on the results of structural analyses and isothermal shrinkage experiments as described in Part III [5]. The predicted plots in fig. 14 show that eq. (4) is not strictly obeyed. These plots are concave so that the values of n derived from the slopes are temperature-dependent varying from approximately $-0.5$ to 0.7 over the temperature range 560 to 600°C. This reflects the fact that the CHR model applies only to the initial stage of sintering since the CHR shrinkage equation is based on the Frenkel model, while the cylinder model describes both the initial and intermediate stages. The shrinkage data obtained for gels by arbitrarily assuming that shrinkage commenced at 525°C are also plotted in fig. 14 for heating rates ranging from approximately 0.5–3.0°C/min. Compared to the behavior predicted by the cylinder model, the values of $Q/(n+1)$ and the heating rate dependence of shrinkage are

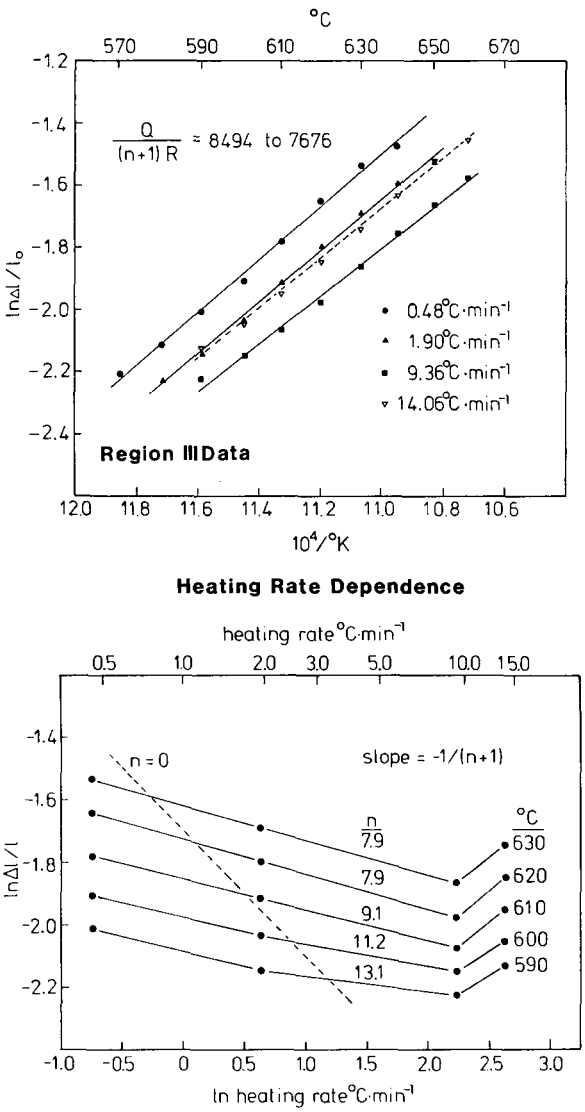


Fig. 15. (a) Ln shrinkage versus $1/T(K)$ plots for Region III calculated using values of total shrinkage. (b) Ln shrinkage versus ln heating rate plots calculated for Region III data (fig. 15(a)). $n$ was determined from the slopes in the interval 0.48 to 9.36°C/min.

considerably less. Figs. 15a and b (plotted without making the assumption that viscous sintering commenced at 525°C and, therefore, using values of total shrinkage) provide the explanation. Values of the slope, $-Q/(n+1)$, are low in part due to the abnormally high values of $n$ which are derived from the plot of ln $\Delta l/l_0$ versus ln(heating rate) (fig. 15b). The values of $-Q/(n+1)$ are higher and the values of $n$ are lower when one assumes shrinkage due to

viscous sintering begins at the beginning of Region III. However, the values of $n$ are still $\gg 0$. For viscous sintering $n$ normally equals zero. In fig. 15b, the values of $n$ determined for heating rates up to 10°C min$^{-1}$ decrease from 13.1 at 590°C to 7.9 at 630°C. High values of $n$ result from a small dependence of shrinkage on heating rate. This behavior can be explained by assuming shrinkage to be proportional to the integral of time divided by viscosity:

$$\frac{\Delta l}{l_0} \propto \int \frac{\mathrm{d}t}{\eta}. \tag{13}$$

As discussed in the previous section, at a particular temperature viscosity increases with the extent of crosslinking and decreases with excess free volume. Shrinkage according to eq. (13) is therefore, promoted by excess free volume and by decreased crosslinking. We have already shown that: (1) increased heating rates reduce the extent of crosslinking which can occur by the beginning of Region III, and (2) structural relaxation may contribute to shrinkage in this Region. Therefore, the small dependence of shrinkage on heating rate in Region III results from the reduction in viscosity for any temperature increment, $\mathrm{d}T$, as the heating rate $\mathrm{d}T/\mathrm{d}t$ is increased. At heating rates up to 10°C min$^{-1}$ this reduction in viscosity with heating rate partly compensates for the reduced time spent at each increment of temperature resulting in high values of $n$. At 15°C min$^{-1}$ the reduction in viscosity is sufficiently large to cause the extent of shrinkage actually to increase with heating rate, thus, changing the sign of $n$. This effect was also observed for alkali-free borosilicate gels [3] and acid catalyzed silica gels [20]. Thus, the large $n$ values result from the time-dependence of $\eta$ that is not accounted for by the CHR model, which assumes that $\eta$ is a single-valued function of $T$. We must conclude, therefore, that it is not possible, in general, to derive meaningful kinetic information from analyses of CHR experiments performed on gels. CHR analyses are valid only if the structure of the polymeric skeleton does not change with temperature. Even in the latter case, it would be more appropriate to use the cylinder model (ref. [28], Appendix 1) which describes the initial and intermediate stages of shrinkage, rather than eqs. (3) and (4), which only apply to the initial stage.

## 4. Summary

We have identified numerous examples in the literature which reveal the inadequacy of the existing models in describing gel densification during the gel → glass conversion and have concluded that it is not correct to consider gel densification basically a sintering process. Actually, at least four mechanisms contribute to shrinkage: (1) capillary contraction due to the increase in surface energy, (2) condensation–polymerization, (3) structural relaxation and (4) viscous sintering. Capillary contraction contributes ~ 3% to the total observed shrinkage and for the borosilicate system investigated is the predominant

shrinkage mechanism below 150°C. Polymerization and structural relaxation result in skeletal densification which closely accounts for the observed shrinkage and reduction in surface area in the temperature range 150–525°C. Skeletal densification which contributes ~ 33% to the total shrinkage, occurs without dramatically changing the local environment of the basic structural units, i.e. the skeletal matrix shrinks isotropically while maintaining the original coordination number of the units which comprise it. Thus, the dimensional scale of motion required for skeletal densification is very small, explaining how this process can occur at quite low temperatures. Sintering accounts for ~ 63% of the total shrinkage and appears to be the predominant shrinkage mechanism above ~ 525°C.

Although we have identified the three temperature regions in which capillary contraction, skeletal densification, and viscous sintering are the predominant shrinkage mechanisms, it is apparent that these regions do not have well-defined boundaries. For example, continued polymerization and structural relaxation strongly influence the sintering kinetics in Region III.

The pathway along which the gel evolves toward a glass is very dependent on thermal history as illustrated schematically in fig. 16. Generally, as the heating rate is increased the low temperature structure is retained to higher temperatures resulting in an enhancement of the densification kinetics. Thus, shrinkage in Regions II and III exhibits a complex heating rate dependence, i.e. although the mechanisms which are responsible for shrinkage are all kinetically limited, the reduced time spent at each increment of temperature as

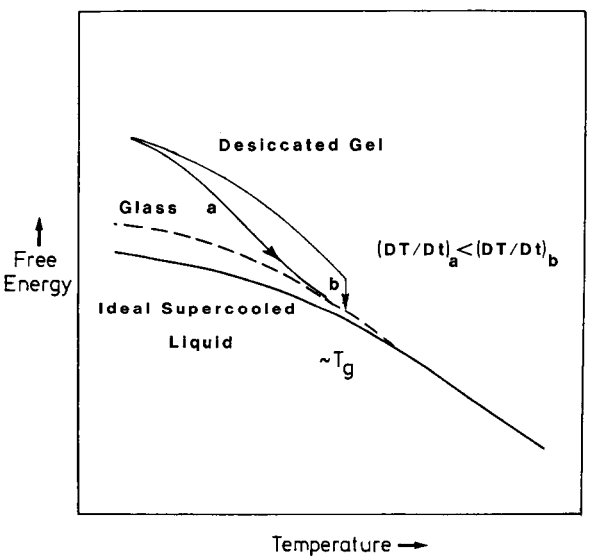


Fig. 16. Schematic representation of free energy changes during the gel to glass conversion. Different pathways illustrate the effect of heating rate.

the heating rate is increased is partly or completely compensated for by increased rates of structural relaxation or viscous sintering. In fact, at sufficiently high heating rates, the reduced viscosity in Region III more than compensates for the reduced time and the gel densification temperature is reduced. This effect (reduction in densification temperature with heating rate) should be very important for gel-derived thin films which can be densified at very high heating rates.

Thermal history also affects the structure of the resulting glass. For example, the heating rate causes differences in the degree of polymerization of the dense glass and may influence the free volume. Therefore, although rapid heating reduces the densification temperature compared to slow heating, it results in a glass with a different structure.

Finally, because of the complex dependence of densification kinetics on heating rate, it appears to be impossible to derive meaningful kinetic information from constant heating rate experiments. Part III of this series [5] describes isothermal shrinkage experiments performed above 525°C (Region III) where viscous sintering is the *predominant* shrinkage mechanism. These experiments illustrate in detail the influence of structural evolution on the mechanism of viscous sintering.

The authors would like to acknowledge the assistance of C.S. Ashley, M.S. Harrington and T.V. Tormey. Discussions with K.D. Keefer and D.W. Schaefer are also appreciated.

## References

[1] C.J. Brinker and G.W. Scherer, J. Non-Crystalline Solids 70 (1985) 301.
[2] J. Zarzycki, J. Non-Crystalline Solids 48 (1982) 105.
[3] C.J. Brinker and S.P. Mukherjee, J. Mat. Sci. 16 (1981) 1980.
[4] C.J. Brinker and G.W. Scherer, Proc. Conf. on Ultrastructure Processing of Ceramics, Glasses, and Composites, Gainesville, FL, February 1983 (Wiley, New York, 1984).
[5] C.J. Brinker, G.W. Scherer and E.P. Roth, J. Non-Crystalline Solids, submitted.
[6] M. Decottignies, J. Phalippou and J. Zarzycki, J. Mat. Sci. 13 (1978) 2605.
[7] R. Jabra, J. Phalippou and J. Zarzycki, J. Non-Crystalline Solids 42 (1980) 489.
[8] P. Murray, E.P. Rodgers and L.E. Williams, Trans. Brit. Ceram. Soc. 53 (1954) 474.
[9] J.K. Mackenzie and R.S. Huttleworth, Proc. Phys. Soc. 62 (1949) 833.
[10] G. Hetherington, K.H. Jack and J.C. Kennedy, Phys. Chem. Glasses 5 (1964) 130.
[11] M. Nogami and Y. Moriya, J. Non-Crystalline Solids 37 (1980) 191.
[12] J. Frenkel, J. Phys. (USSR) 9 (1945) 385.
[13] W.S. Young, S.T. Rasmussen and I.B. Cutler in Ultra-Fine Grain Ceramics, eds., J.J. Burke, N.L. Reed and V. Weiss (Syracuse Univ. Press, Syracuse, NY, 1970).
[14] W.S. Young and I.B. Cutler, J. Am. Ceram. Soc. 53 (1970) 659.
[15] J.L. Woolfrey and M.J. Bannister, J. Am. Ceram. Soc. 55 (1972) 390.
[16] M.J. Bannister, J. Am. Ceram. Soc. 51 (1968) 548.
[17] R.K. Iler, The Chemistry of Silica (Wiley, New York, 1979).
[18] G.W. Scherer and M.G. Drexhage, J. Am. Ceram. Soc. to be published.
[19] G.W. Scherer, J. Am. Ceram. Soc. 60 (1977) 236.
[20] C.J. Brinker, G.W. Scherer and W.D. Drotning, in: Better Ceramics Through Chemistry, eds., C.J. Brinker, D.E. Clark and D.R. Ulrich (Elsevier–North-Holland, New York, 1984).

[21] N. Tohge, G.S. Moore and J.D. Mackenzie, Proc. 2nd Int. Workshop on Gels, Wurzburg, W. Germany, June 30–July 1, 1983, J. Non-Crystalline Solids 63 (1984) 95.
[22] C.J. Brinker, K.D. Keefer, D.W. Schaefer and C.S. Ashley, J. Non-Crystalline Solids 48 (1982) 47.
[23] S.M. Rekhson et al., Sov. J. Inorg. Mat. 7 (1971) 622.
[24] T.A. Gallo, C.J. Brinker, L.C. Klein and G.W. Scherer, in: Better Ceramics Through Chemistry, eds., C.J. Brinker, D.E. Clark and D.R. Ulrich (Elsevier–North-Holland, New York, 1984).
[25] J.P. Williams, Am. Ceram. Soc. Bull. 55 (1976) 524.
[26] G. Gibbs, private communication.
[27] B.A. Morrow and L.A. Cody, J. Phys. Chem. 80 (1976) 2761.
[28] G.W. Scherer, J. Am. Ceram. Soc. 60 (1977) 236.